Journal of Solid State Chemistry 183 (2010) 2227–2235

Contents lists available at ScienceDirect

Journal of Solid State Chemistry

journal homepage: www.elsevier.com/locate/jssc

Structural investigation in the TiB_2–($Na_2O \cdot B_2O_3 \cdot Al_2O_3$) system

Elena Buixaderas [a,*], Elena Maria Anghel [b,1], Simona Petrescu [b], Petre Osiceanu [c,2]

[a] Institute of Physics, Academy of Science of the Czech Republic, Dielectrics Department, Na Slovance 2, 18221 Prague 8, Czech Republic
[b] Institute of Physical Chemistry "Ilie Murgulescu"of Romanian Academy, Molten Salts Department, Spl. Independentei 202, 060021 Bucharest, Romania
[c] Institute of Physical Chemistry "Ilie Murgulescu" of Romanian Academy, Laboratory of Catalysis and Surface Chemistry, Spl. Independentei 202, 060021 Bucharest, Romania

ARTICLE INFO

Article history:
Received 3 May 2010
Received in revised form
8 July 2010
Accepted 14 July 2010
Available online 18 July 2010

Keywords:
Composite
Self-propagating high-temperature synthesis
Structure
Raman
X-ray photoelectron spectroscopy

ABSTRACT

Composites in the TiB_2–$Na_2O \cdot B_2O_3 \cdot Al_2O_3$ systems, TiB_2–MBA (MB stands for sodium metaborate and A is Al_2O_3), were prepared by self-propagating high-temperature synthesis (SHS), in simultaneous mode. Selection of these compositions was ruled by the interesting properties of both TiB_2 and double borates of alkali metal and aluminum. The structure of the obtained materials was evaluated by micro-Raman spectroscopy, from room temperature up to 600 °C, and X-ray photoelectron spectroscopy (XPS). Formation of the TiB_2 and $TiO_{2-x}B_x$ phases along with TiO_2 as rutile were identified as titanium speciation in the grain phase embedded in a sodium aluminum borate matrix. Integration of the Raman spectra of the grain phases revealed a TiB_2 content of 16.99% and 23.32% for the two composite investigated $2TiB_2 \cdot 2MBA$ and $3TiB_2 \cdot 5MBA$. A constrained-width model for the spectral deconvolution of the high-frequency Raman band was forwarded to calculate the proportion of tetrahedral boron atoms (7.424%) in the blank borate matrix $Na_2B_2O_4 \cdot Al_2O_3$ in solid phase.

1. Introduction

Owing to their very interesting properties—UV transparency, high polarizability, resistance against radiation-induced damages, unusual transport properties (electronic and ionic)—oxyborate systems are promising candidates for non-linear optical materials with harmonic generation applications, lithium-ion battery electrodes, ion conductors as well as separation and storage media, and catalysts [1,2]. The latter applications are encountered when tunnel structures are present. On the other hand, combining these double borates with TiB_2 (melting point of about 3225 °C, heat conductivity of 24–59 $W\,m^{-1}C^{-1}$, electrical resistivity of 20.4 μΩ cm and hardness of 2500 Kg/mm^2 for > 95 dense at 25 °C [3]) is expected to trigger an intricate change of properties.

Preparation of the TiB_2-based composite by self-propagating high-temperature synthesis (SHS) was proven to be an efficient, inexpensive, time, and energy saving method [3–7] in comparison to the sintering method and melting-casting route. Besides due to its hexagonal symmetry TiB_2 is difficult to sinter without micro-cracking [3]. The SHS process consists in a highly exothermal reaction within a mixture of reactant powders that allow obtaining of high temperature ceramics and composite materials, typically with high porosity of about 50%. Composites like crystalline TiB_2 inserted in the aluminoborate glassy matrix, TiB_2–(MO–Al_2O_3–B_2O_3) (M stands for Ba, Mg, Ca), were designed for applications where strength, hardness, and electrical conductivity are required [4], while porous composites from the TiB_2–(Al_2O_3–CaO) systems are candidates for infrared light transmission applications [5]. Electrical properties of the TiB_2-containing materials were extensively investigated due to its possible use as electrode materials for aluminum electrosynthesis [3].

Tailoring materials for certain applications by understanding their microstructure-physical properties correlation is a major challenge for physics as well as for material science. Conversely, this work aims to characterize structure on different scales combining X-ray photoelectron spectroscopy (XPS), and Raman spectroscopy of the TiB_2–($Na_2O \cdot B_2O_3$–Al_2O_3) composites prepared by SHS in simultaneous mode.

2. Experimental

2.1. Materials

Titanium dioxide TiO_2 of 99% purity (Merck), aluminum Al powder with average size of 25 μm (97% purity supplied by Aluminum Slatina, Romania), boric oxide B_2O_3 of 99.93% purity (Merck), aluminum oxide Al_2O_3 powder with 0.063–0.2 range size (Merck), and Na_2CO_3 of 99.8% purity (Reactivul Bucharest) were used as raw materials (see details in Table 1). TiB_2 powder of

* Corresponding author. Fax: +420 286 890 415.
E-mail addresses: buixader@fzu.cz (E. Buixaderas), manghel@icf.ro (E. Maria Anghel), posic@icf.ro (P. Osiceanu).
[1] Fax: +4021 312 11 47.
[2] Fax: +4021 312 11 47.

0022-4596/$ - see front matter © 2010 Elsevier Inc. All rights reserved.
doi:10.1016/j.jssc.2010.07.023

Table 1
Nominal compositions of the reactant powders, yielding reactions of the TiB_2–$Na_2Al_2O(BO_3)_2$ composites with various molar ratios: B_2O_3/TiO_2 (R).

Sample	TiO_2	Al	Al_2O_3	Na_2O[a]	$Na_2B_4O_7$	B_2O_3	Reaction	R
MB	–	–		50	–	50	$Na_2CO_3+B_2O_3 \rightarrow Na_2B_2O_4+CO_2$	-
MBA	–	–	33.3	33.3	–	33.3	$Na_2CO_3+B_2O_3+Al_2O_3 \rightarrow Na_2B_2O_4 \cdot Al_2O_3+CO_2$	-
2MB	25	50		–	25	–	$2TiO_2+2Na_2B_4O_7+4Al \rightarrow 2TiB_2+2(Na_2O \cdot B_2O_3 \cdot Al_2O_3)+2O_2$	0.67
5MB	11.53	38.48		19.23	–	30.76	$3TiO_2+5Na_2CO_3+8B_2O_3+10Al \rightarrow 3TiB_2+5(Na_2B_2O_4.Al_2O_3)+5CO_2$	2.66

[a] Na_2CO_3 was the source for Na_2O.

10 μm with 98% purity (Aldrich) and the prepared borate matrices according to the Na_2O–Al_2O_3–B_2O_3 phase diagram [1,8], i.e. $Na_2B_2O_4$ and $Na_2B_2O_4 \cdot Al_2O_3$, were used for comparative purposes. The B_2O_3/TiO_2 molar ratio of the reactant powders was taken into consideration for selection of the two compositions in Table 1, 2MB and 5MB respectively, knowing the fact that at a higher ratio than 1 formation of the Al_3Ti phase is hindered [6]. Also two different boron- and sodium-containing reactants, $Na_2B_4O_7$ ($Na_2O \cdot 2B_2O_3$), and Na_2CO_3 along with B_2O_3, were employed in preparation to avoid CO_2 retention that can give severe preparative problems [9]. Reactant mixtures were weight, homogenized for 2 h in the ball mill with acetone, dried, pressed into disk shape up to 40–60% of theoretical green densities. The resulted pellets were heated up equally, simultaneous ignited, in a preheated furnace within 1000–1200 °C temperature range, in air. Thus, the non-equilibrium condition of the SHS of the high heating rate was achieved. However, the self-sustaining combustion temperature, T_c, was not measured. High temperature combustion enables volatilization of the impurities.

2.2. Raman spectroscopy

Unpolarized solid state Raman spectra were recorded over 10–900 cm^{-1} and 200–1800 cm^{-1} using a RM-1000 RENISHAW Raman Microscope, equipped with a charge coupled device (CCD) detector, and a Leica microscope with a 50× objective, in backscattering geometry. The emission line at 514.532 nm of an Ar^+ laser was used to excite the samples at 25 mW power. The diameter of the laser spot on the sample surface amounted to 2–3 μm providing a spectral resolution better than 2 cm^{-1}. A THMS-600 cell (LINKAM) was used for temperature control of the samples from 25 to 600 °C with an accuracy of the 0.1 °C.

Approximately 70 Raman spectra were acquired at room temperature on the 5MB polished disk by in-line scanning with a spatial resolution of 1 μm to study sample homogeneity.

Raman spectra collected at different temperatures were temperature-reduced to account the first order Bose–Einstein distribution factor [10]. The reduced spectra were obtained from the experimental spectra, $I_{exp}(\upsilon)$ as following:

$$I_R(\nu) = I_{exp}(\nu)\frac{1-e^{-h\nu/k_BT}}{(\nu_0-\nu)^4}\nu \quad (1)$$

where υ is the frequency of the Raman shift and $n(\upsilon,T)$ represents the Bose–Einstein population factor with $n(\upsilon)=[\exp(\hbar\upsilon/k_BT-1)]^{-1}$. The $\hbar$ and k_B are Plank and Boltzmann constants. Then a multicomponent fit was performed by Igor Software. Cubic baseline correction was performed for the glassy $Na_2B_2O_4 \cdot Al_2O_3$ sample while the background for each spectrum of the SHS composites was subtracted by using linear segments as described by Robinet et al. [11]. Gaussian distributions [10] were used to model the band shapes of the Raman spectra.

2.3. Differential thermal analysis (DTA)

The crystallization behavior of $Na_2B_2O_4 \cdot Al_2O_3$ glass was also monitored using a DTA instrument METLER Star SW 9.00 with a heating rate of 10°/min under nitrogen atmosphere.

2.4. X-ray photoelectron spectroscopy (XPS)

Surface analysis performed by XPS was carried out on VG Scientific ESCALAB 250 system, with a base pressure in the analysis chamber of 10^{-9} Torr. The X-ray source was Al$K\alpha$ radiation (1486.6 eV, monochromatized) and the overall energy resolution is estimated at 0.7 eV by the full width at half maximum (FWHM) of the Au4$f_{7/2}$ line. The spectrometer was calibrated by assuming that the binding energies (BEs) of Au4$f_{7/2}$ is 84 eV, $Ag_{5/2}$ line is 368.27 eV, and Cu2$p_{3/2}$ line is 932.67 eV with respect to the Fermi level according to Antony [12]. The standard deviation in the BE values is lower than 0.2 eV. To avoid further carbon and oxygen contamination of the samples, a small piece of couple millimeters was investigated by XPS. Survey scans (0–1100 eV) were recorded for each sample in order to evidence all the XPS features of the elements found out on the surface. Subsequently, high resolution scans over narrow energy ranges were recorded around each peak of interest. Raw spectra were smoothed and fitted with a non-linear least-square fit program using Gauss–Lorentzian peak shapes after the linear background subtraction. The fitting procedure included four parameters: peak position, full width at half maximum (FWHM), Gaussian–Lorentzian mixture ratio, and intensity ratio constraints.

To take into account the charging effect of the measured binding energies (BEs) the spectra were calibrated using the C1s line (BE=284.8 eV) of the adsorbed hydrocarbon on the sample surface.

3. Results and discussion

3.1. Raman spectra

Raman spectroscopy is a very useful technique in studying chemical structure and morphology of the heterogeneous materials as composites under discussion.

3.1.1. Sodium aluminum metaborate matrix

For comparative purposes, reduced representations of the unpolarized Raman spectra of the crystalline sodium metaborate compound, $Na_2B_2O_4$ (MB), and the sodium aluminum metaborate glass, $Na_2B_2O_4 \cdot Al_2O_3$ (MBA), which represents the blank matrix of the TiB_2–($Na_2B_2O_4 \cdot Al_2O_3$) composites are illustrated in Fig. 1a up to 577 °C, in the same spectral range. Results of the spectral deconvolution and their assignments for room temperature Raman spectra were summarized in Table 2. Table 3 includes temperature-dependent structural changes of the MBA

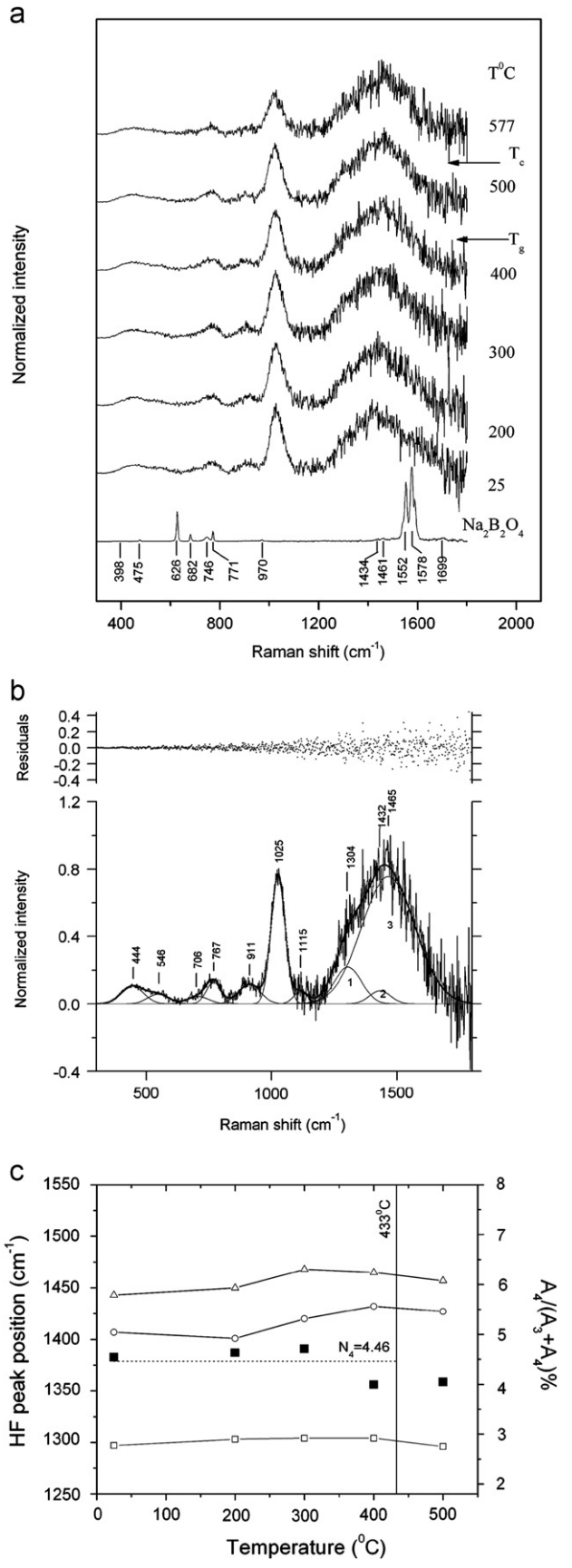

Fig. 1. Temperature-reduced unpolarized Raman spectra of $Na_2B_2O_4 \cdot Al_2O_3$: (a) within 25–577 °C (the glass transition T_g is 433 °C and the onset crystallization temperature is 562 °C), (b) deconvoluted spectrum collected at 400 °C (with three-component deconvoluted HF band), (c) positions of the HF peaks and calculated N_4 (solid square).

composition up to 577 °C which is simplified and is shown in Fig. 1b for 400 °C.

Alkali borate glasses show the so-called boron anomaly since their physico-chemical properties (e.g. density and thermal expansion coefficient) have a minima or maxima according to their composition or to the proportion of boron atoms in three- and/or 4-fold coordination [13–18]. The two types of the boron atoms constitute non-ring and ring groups. Particularly metaborate chemistry is described by izomerization reaction between metaborate triangle $B\O_2O^-$ and tetrahedral $B\O_4^-$ units ($B\O_2O^- \Leftrightarrow B\O_4^-$) depending on the type of cation and temperature [14]. For instance Raman spectrum of the sodium metaborate compound (called MB in Fig. 1a) revealed that all boron atoms are placed in triangular arrangements [19] while simulated magic angle spinning (MAS) NMR found a 3.6% of boron atoms in tetrahedral arrangements [20].

Although there are various ways to divide Raman spectra of the alkali borate glasses [10,13,14,21] our spectra were discussed in terms of three regions: low ($<600\ cm^{-1}$), middle (600–1140 cm^{-1}), and high-frequency regions ($>1140\ cm^{-1}$) to include the anti-symmetric stretching band of the tetrahedral boron atom–oxygen, B(4)–O, at 1139 cm^{-1} [13,22]. Each of these regions can be subdivided. Thus, in the low frequency (LF) region (above 300 cm^{-1}) the bending vibrations of tetrahedral boron atoms, $\delta_{B(4)-O}$, are shifted towards a higher frequency than the triangular counterparts [13,14]. Mid-frequency (MF) region consists in a spectral domain up to 900 cm^{-1} for B(4)–O stretching vibrations and the other domain above 900 cm^{-1} for B(3)–O stretching vibrations of the trigonal boron atoms [13]. If the MF envelope is related to the ring-type superstructures and defines the intermediate range order, the high-frequency envelope is assignable to the stretching of the $B–O^-$ bonds attached to large borate groups and represents short-range order (Table 2) [21].

Fig. 1a shows influence of the Al_2O_3 addition on the structure of the crystalline $Na_2B_2O_4$ (MB) concerning position and width of the Raman features of the sodium boroaluminate glass, MBA. Its LF region at room temperature is dominated by a broad band peaking up at about 442 cm^{-1} and with a shoulder at around 560 cm^{-1}. Precise assignment of these bands was not offered in the literature but they might be originated from destruction of large, connected groups [17], and/or to the Al–O stretching modes in AlO_6 groups modes coupled with the borate vibrational modes [14]. It is well known that Al_2O_3 in borate glasses, Al^{3+} can adopt either: six-, five-, and/or four-coordination [22]. If six-fold aluminum groups give Raman bands in the low frequency region, four-coordinated aluminum groups will influence MF bands of the borate glasses. Besides, moderately modified borate compounds as alkali earth metaborate ones, $MeO \cdot B_2O_3$ (*Me* stands for Li, Ca, Sr), show a band at 550 cm^{-1} which denotes the presence of BO_4 units in "loose" groups [15], i.e. pentaborate and tetraborate groups [14], as a result of depolymerization of large network segments.

The next region (MF), within 25–577 °C temperature range, was deconvoluted into five bands as pointed in Table 3 and illustrated in Fig. 1b for 400 °C. Although both MB and MBA have the band at about 770 cm^{-1} much wider band for MBA (57 cm^{-1} in comparison to 9.7 cm^{-1}) point out different origin of the two bands. On the whole a Raman band located at about 770 cm^{-1} for borate glasses does not indicate the presence of particular ring-like group; hence, it is generically named boroxy ring [15,17] with one BO_4 (see Table 2) while for crystalline compounds as MB where no BO_4 units were depicted [19] this band is much narrower. Slight decrease in the intensity of the band at about 772 cm^{-1} when temperature increases signals that the interconnected boroxy rings (772 cm^{-1} band) start "loosing" (560 cm^{-1}) and breaking up (high frequency bands within

Table 2
Raman bands and their assignment for the sodium metaborate coumpound and the sodium aluminum metaborate glass collected at room temperature.

$Na_2B_2O_4$ (MB)	$Na_2B_2O_4 \cdot Al_2O_3$ (MBA)	Assignment	Literature value (cm^{-1})	References
Low frequency			<600	[13]
398	–	Bending of the O–B(3)–O bonds	350–600	[14]
–	451	Al–O stretching modes of the isolated AlO_6 units	400–530	[14]
475	–	Bending vibrations of the BO_3 units with all bridging oxygens	475	[14]
–	560	Bending vibrations of the BO_4 units in dismantled network and Al–O–Al bending between $Al\emptyset_4^-$ units	555 and 550	[14–16]
Mid-frequency		*Intermediate range order*	600–1140	[13,14]
626	–	Breathing vibration of the metaborate ring (B_3O_9) and involves displacement of both rings and non-bridging oxygens	627	[15]
682	–	Ring torsion vibration	690	[16]
746	732	Out-of-plane bending mode of metaborate triangles	700–800	[14]
771[a]	–	Out-of-plane bending mode of metaborate triangles	700–800	[14]
	772	Planar six-membered rings with one BO_4 units (i.e. metaborate ring) and AlO_4 units bonded to NBO	770 and 780	[15,16]
970	911	Symmetric stretching of the B(3)-O bonds	900–1000	[13]
–	1030	Asymmetric stretch of the $Al\emptyset_4^-$ units linked to $B\emptyset_2O^-$ units and/or symmetric stretching of the CO_3^{2-} anions	950–1000 and 1060	[14,15]
–	1138	Units containing both metaborate triangles and tetrahedra	1100	[14]
High frequency		*Short range order*	>1140	[13,14]
–	1297	Stretching modes of $B\emptyset_2O^-$ linked to $Al\emptyset_4^-$	1340–1390	[14]
–	1407	Stretching vibrations of the $B\emptyset_2O^-$ linked to $B\emptyset_4^-$	1400–1420	[14]
1434, 1461, 1500	1443	Stretching modes of the $B\emptyset_2O^-$ linked to $B\emptyset_2O^-$	1450–1500	[14]
1542, 1552, 1578	–	Symmetric stretch of the $B–O^-$ of large borate groups and E_{2g} mode of the grafitic materials	1500 and 1580	[17,18]
1692	1633	Bending of H–O–H bonds	1638	[13]

B(4) and B(3) denote the tetrahedral and trigonal boron atoms.

[a] Its full-width at half maximum (FWHM) is 9.7 cm^{-1}.

1240–1650 cm^{-1}). The two processes of borate network dismantling are usually enhanced during melting and less pronounced in solid state up to the glass transition (T_g of 433 °C). The presence of diborate rings B_4O_9 (signaled by the concomitant presence of the bands: 500, 770, 930, and 1120 cm^{-1}, out of them 500 and 930 cm^{-1} represent loose diborate rings [15]) is ruled out in $Na_2B_2O_4 \cdot Al_2O_3$. Tetraborate rings, B_8O_{16} meaning a triborate ring (B_3O_7) linked to a pentaborate ring (B_5O_{10}), with bands at 520, 670, and 975 cm^{-1}, are formed in this glass.

Yet Al_2O_3-induced modifications of the borate glass structure consist in formation of the $Al\emptyset_4^-$ (Raman band at about 780 cm^{-1}) [14] concurrently with lowering concentration of the tetrahedral boron atoms (band at about 735–770 cm^{-1}) [15,17] and gradual conversion of the boroxy rings to the boroxol rings (806 cm^{-1}) [23,24], no obvious presence of the band at 806 cm^{-1} (B_3O_6) was noticed in Fig. 1. Hence changing of the proportion of B(4), N_4, is the only indirect validation on the $Al\emptyset_4^-$ presence in the MBA glass. Two plausible explanations of the alumina influence on the borate matrix are supplied by NMR data in literature [25–27]. The first one relies on the charge compensation of the $(MO_4^-)Na^+$ units (M=Al and/or B), where the sodium compensated AlO_4^- units have the precedence over boron ones since Al_2O_3 is more acidic than B_2O_3 [25]. Although small quantities of alumina reacts with Na_2O to form AlO_4^- species compensated by Na^+, high quantities of alumina might cause phase separation due to the fact that scarce quantities of Na_2O are not able to dissolve high field cations (like Al^{3+}) and then phase separation occurs. The second interpretation consists of boron and aluminum competition for oxygen and preference of oxygen for the higher field atom (in this case Al^{3+}) as well as of tetrahedral avoidance [26,27], i.e. formation of the Al(4)–O–B(4) bonds between tetrahedral aluminum and boron atoms through oxygen bridges are less probable to take place. Despite the fact that aluminum borosilicate and fluoroborate glasses [26,28] contain mostly 4-fold coordinated aluminum units, 5- and 6-fold coordinated units are also present. The latter ones are isolated in clusters.

The unsolved strong band at 1029 cm^{-1} might be assigned to the CO_3^{2-} ions [15] from Na_2CO_3 used for preparation (see Table 1). In highly modified borate glasses CO_2 retention causes serious preparative problem with implications on viscosity-related glass transition temperature [9] and give a narrow (FWHM of about 35 cm^{-1}) strong Raman band at about 1060 cm^{-1}. However, the much wider band at 1030 cm^{-1} could originate from network-forming structural units as AlO_4^- connected with $B\emptyset_2O^-$ [14].

The third region, HF, of the Raman spectra of the aluminoborate glasses originates from the stretching modes of the $B\emptyset_2O^-$ arrangements [14]. Although couple deconvolution models of the HF bands [10,21,24] were attempted for the alkali borate glasses, number of the components and their assignments are still a matter of debate. Despite the numerous component models some of the close bands have the same origin as the bands four and six ($B\emptyset_2O^-$ units) of the model forwarded by Yano et al. [21] of the $Na_2O–B_2O_3$ glasses with 36% Na_2O. Chryssikos et al. [14] divided the HF of the lithium metaborate-metaaluminate crystals into three ranges within 1340–1500 cm^{-1}; model assimilated for deconvolution of the MBA glass (Table 2). Although first range, 1340–1390 cm^{-1}, is somehow shifted towards higher frequency than the band at 1297 cm^{-1} found in case of MBA at room temperature; however high Al_2O_3 additions (50% in MBA) can trigger such behavior and/or contribution of the $B\emptyset O_2^{2-}$ units should be considered. Relative areas of the second and third bands in the 1400–1420 cm^{-1} and 1450–1500 cm^{-1} give indirect information about proportion of the tetrahedral boron atoms, N_4, and the trigonal boron atoms, N_3, respectively (see Fig. 1b and Table 3). Given the fact that these relative integrated intensities are almost insensitive to the temperature change up to the glass transition [10] (in this case T_g is 433 °C), we made the assumption that bandwidth of the second and third bands from HF region were kept constant up to 500 °C; hence, N_3 and N_4 to be in agreement with NMR data in literature [20,29]. For instance Bertmer et al. [20] found a N_4 of 4.2% for a similar

Table 3
Results (peak position, width, area) of the deconvolution procedure of the Raman spectra for the $Na_2B_2O_4 \cdot Al_2O_3$ solid collected at various temperatures.

	Temperature (°C)				
	25	200	300	400	500
Peak (cm^{-1})	451	451	438	444	443
FWHM (cm^{-1})	115	113	98	107	105
Peak (cm^{-1})	560	553	534	546	541
FWHM (cm^{-1})	85	73	100	99	91
Peak(cm^{-1})	732	680	714	706	729
FWHM (cm^{-1})	130	125	121	100	167
Peak (cm^{-1})	772	763	771	768	767
FWHM (cm^{-1})	57	74	65	68	62
Peak (cm^{-1})	911	913	907	911	907
FWHM (cm^{-1})	77	656	78	104	77
Peak (cm^{-1})	1030	1029	1027	1025	1024
FWHM (cm^{-1})	65	70	69	65	68
Peak (cm^{-1})	1138	1141	1141	1115	1137
FWHM (cm^{-1})	56	62	68	66	43
Peak (cm^{-1})	1297	1303	1304	1304	1296
FWHM (cm^{-1})	85	66	115	127	81
Peak (cm^{-1})	1407	1401	1420	1432	1427
FWHM (cm^{-1})	100	100	100	100	100
A_4	*9.229*	*8.876*	*10.124*	*8.373*	*8.515*
Peak (cm^{-1})	1443	1450	1468	1465	1457
FWHM (cm^{-1})	250	250	250	250	250
A_3	*193.92*	*182.600*	*204.69*	*209.713*	*201.620*
$A_4(A_3+A_4)$	*0.0454*	*0.0463*	*0.0471*	*0.0399*	*0.0405*
Peak (cm^{-1})	1633	–	–	–	–
FWHM (cm^{-1})	125	–	–	–	–

FWHM is full-width at half maximum, underlined values were kept constant during the fit.
A_3 and A_4 are areas that denote the B(4) and B(3) content.

composition: $35Na_2O{:}35B_2O_3{:}30Al_2O_3$ with the same Na/B ratio as in MBA. Our calculations show a mean value of 4.46% $B\emptyset_4^-$ tetrahedral (Fig. 1c).

Lack of the concomitant presence of the 588, 895, and 1275 cm^{-1} bands in the investigated MBA glass infirm the presence of the orthoborate units charge-balanced by Na^+. In fact triangular arrangements of the boron atoms consist in the metaborate and/or pyroborate units, $B\emptyset_2O^-$ and/or $B\emptyset O_2^{2-}$ units.

Splitting of the HF band for glassy sodium aluminum metaborate above glass transition, the 577 °C spectrum (Fig. 1a), is a manifestation of the crystallization process started at 562 °C, the onset temperature of the exothermal peak of crystallization at 607 °C. Besides increased intensity of the HF band evidencing short range order, contrary to the bands around 770 and 1030 cm^{-1} which defines medium range order, indicates the beginning of the glass network depolymerization of the MBA.

3.1.2. TiB_2–MBA composites

Reduced Raman spectra of the two TiB_2-containing composites, $3TiB_2 \cdot 5MBA$ and $2TiB_2 \cdot 2MBA$ (where MBA is $Na_2B_2O_4 \cdot Al_2O_3$), named 5MB and 2MB, and the corresponding micrographs for the 2MB composite obtained by the SHS reactions (Table 1) are shown in Fig. 2. Limited spectral range, in the 20–870 cm^{-1} range, was chosen in accordance with the fact that Raman bands of TiB_2 and TiO_2 (all polymorph forms) [30,31] are located below 650 cm^{-1}. Since these composites are constituted by a grain phase and a borate matrix which accommodate grains or intergrains phase (see micrographs in Fig. 2a for the 2MB composite), their Raman spectra are exemplified according to the grain and intergrains phases and compared with Raman spectra of commercial TiB_2 powder for grain phase and with sodium aluminum metaborate matrix, previously described.

The microstructure of the grain phase in the 2MB sample at room temperature and at 590 °C (Fig. 2a) is prismatic-type one similar to the TiC/TiB_2 composites as reported by Vallauri et al. [3].

Although a simplified model of deconvolution might have been chosen for the Raman spectra of the grain phase, however to account for the TiB_2 content, all components of the Raman spectrum of single TiB_2 were reproduced. Results of the deconvolution procedure of the grain phase spectra of the two composites 2MB and 5MB are listed in Table 4. Based on Raman data reported in literature [30,31] for TiB_2 containing composites and for TiO_2 as rutile and anatase polymorphic forms, reduced spectra of the grain phase is summation of the TiB_2 and rutile spectra as illustrated in Fig. 3 for the 5MB composite. Proportion of TiB_2 in the two composites 2MB and 5MB calculated by spectra integration was found to be 15.11% and 32.51%, respectively. Thus, the grain phases, crystalline phases (with relatively narrow Raman bands), investigated here are mostly rutile. These proportions are somehow conflicting to the ones predicted by reactions in Table 1, 50% for 2MB and 37.5% for 5MB. A plausible cause of this behavior can be the different precursors of Na_2O and B_2O_3 used in preparation. But other factors that control SHS process (powder size, homogenization conditions, combustion temperature, duration, etc.) are not to be discarded.

As the temperature increases, the positions of the two peaks of rutile, 447 and 608 cm^{-1}, are shifted towards lower wavenumbers, 411 and 600 cm^{-1} due to thermal expansion (see Fig. 2). No considerable increase of the band intensities related to TiO_2 as oxidation product of TiB_2 and 2MB and 5MB were noticed up to 590 °C.

The spectral in-line scan within 70 μm, employed to probe the homogeneity of the 5MB composite, is presented in Fig. 4. It shows that TiB_2 and rutile, with strong Raman features below 650 cm^{-1}, are embedded unevenly in the borate matrix or intergrains phase, with spectral features up to 1600 cm^{-1}. Some spectra are contaminated by fluorescence or another sloping baseline. Bose–Einstein reduced spectra, after the fluorescent baseline correction, for the intergrains phase of the 5MB composite are displayed in Fig. 5 and reveal a complex structure of the borate matrix (Table 5), and are different from those of the crystalline MB and glassy MBA (inset of Fig. 5). Narrower and split bands of the intergrains spectrum imply less disorder or more crystalline character of the 5MB intergrains phase in contrast to the blank MBA. Asymmetric band peaking up at about 802 cm^{-1} along with 1259 cm^{-1} give evidence of the boroxy ring conversion to the boroxol rings [23,32] under Al_2O_3 influence. Boroxol rings are the main constituents, more than 70%, of the single B_2O_3 glass. Very intense band at about 1598 cm^{-1} might point out formation of crystalline $Na_2B_2O_4$. However, the absence of the very intense band at 626 cm^{-1} specific to crystalline $Na_2B_2O_4$ (see Fig. 1) might signal presence of a non-crystalline sodium metaborate phase. Also it is well known that water and carbon contamination [13,18] cause a significant enhancement of the Raman bands in the high frequency region and fluorescent background as noticed in Fig. 4. Contaminant effects (fluorescence

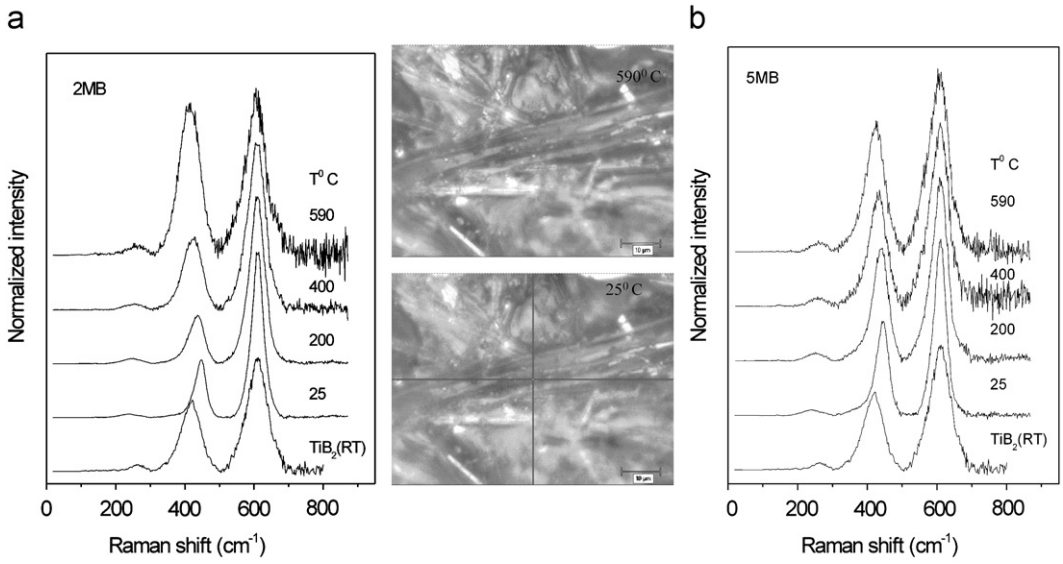

Fig. 2. Temperature-reduced Raman spectra of the grain phase in (a) 2MB composite with its Raman micrographs collected at room temperature and 590 °C (middle position of the micrographs are the spots were Raman spectra were collected) and (b) 5MB composite.

Table 4
Results of the deconvolution procedure of the room temperature Raman spectra of the grain phase and their literature assignments for 2MB and 5MB mixtures.

2MB			5MB			Assignment	Literature value (cm^{-1})	References
Peak (cm^{-1})	FWHM (cm^{-1})	Area (cm^{-2})	Peak (cm^{-1})	FWHM (cm^{-1})	Area (cm^{-2})			
232	60	1.1217	232	56	1.405	TiO_2	238	[28]
262	50	0.21672	262	50	0.55201	TiB_2	260	[27]
358	53	0.26729	358	53	0.68072	TiB_2		[28]
419	66	3.1692	419	66	8.0727	TiB_2	409	[27]
445	37	12.024	446	38	17.328	TiO_2	447	[28]
609	43	39.61	608	39	30.934	TiO_2	611	[28]
609	76	5.7402	609	76	14.62	TiB_2	598	[27]
% TiB_2		15.11			32.51			

Peak parameters (position and corresponding FWHM) for TiB_2 were kept constant during the fit in order to reproduce its spectrum.

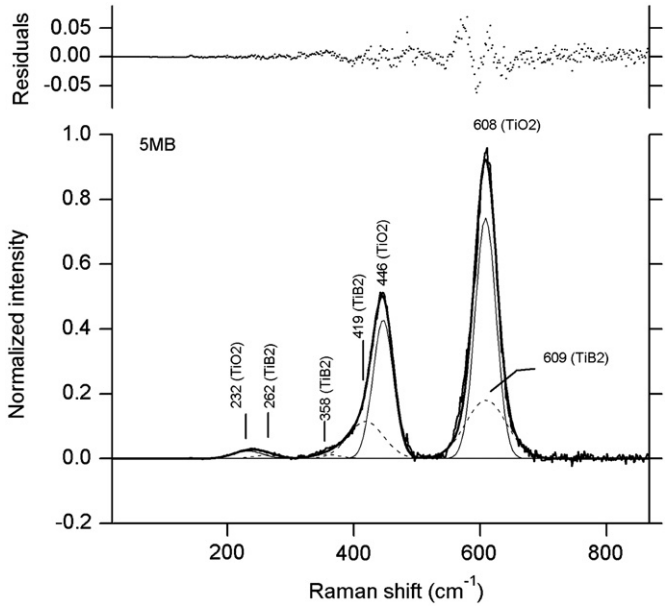

Fig. 3. Deconvoluted Raman spectrum of the grain phase of the 5MB composite.

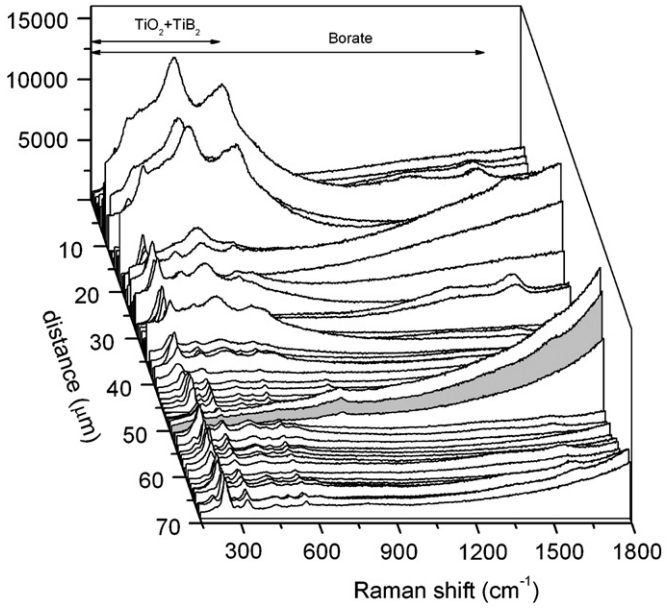

Fig. 4. Spectral in-line scan (1 μm step) of the 5MB composite, cross section.

Table 5
Results of the deconvolution procedure of the Raman spectra of the intergrains phase and the literature assignment for the 5MB composite at room temperature.

Peak (cm^{-1})	FWHM (cm^{-1})	Assignment	Literature value (cm^{-1})	References
261	25	TiB_2	260	[30]
339	17	TiB_2	358*	
417	6	TiB_2	409, 419*	[30]
500	30	Bending B(4)–O (BO_4 groups resulted from depolymerized large groups as pentaborate and tetraborate rings)	490–570	[13]
553	45	Bending vibrations of the BO_4 units in dismantled network and Al–O–Al bending between $AlØ_4^-$ units	555 and 550	[14–16]
595	57	TiB_2	598	[30]
762	72	Planar six-membered rings with one BO_4 units (i.e. metaborate ring) and AlO_4 units bonded to NBO	770 and 780	[15,16]
802	34	Boroxol rings (B_3O_6)	805	[23]
848	44	Pyroborate units (B_2O_5)	820	[15]
896	32	TiO_4 in borate matrix	900	[22]
974	67	Symmetric stretching of the B(3)–O bonds	900–1000	[13]
1039	15	Stretching modes of boron tetrahedra and/or symmetric stretching of the CO_3^{2-} anions	1050 and 1060	[14,15]
1150	140	Anti-symmetric stretching of the B(4)–O bonds	1139	[13]
1259	60	Boroxol rings (B_3O_6)	1260	[23]
1345	49	Stretching modes of $BØ_2O^-$ linked to $AlØ_4^-$	1340–1390	[14]
1406	52	Stretching vibrations of the $BØ_2O^-$ linked to $BØ_4^-$	1400–1420	[14]
1496	51	Stretching modes of the $BØ_2O^-$ linked to $BØ_2O^-$	1450–1500	[14]
1598	64	Stretching of the B–O^- linked to large borate groups (crystalline sodium metaborate) and E_{2g} mode of the grafitic materials	1575 and 1580	[15,18]
1615	29	Bending of H–O–H bonds	1638	[13]

* Asterisk denotes present work.

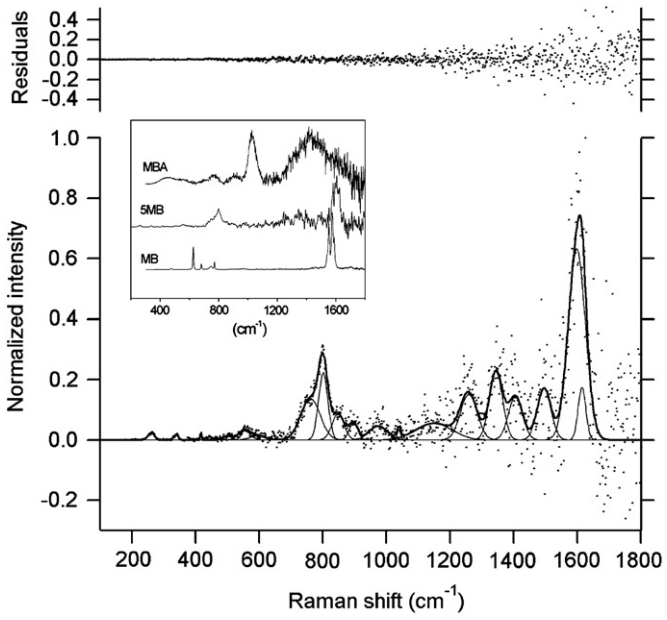

Fig. 5. Deconvoluted Raman spectra of the intergrains phase in 5MB composite. Inset is the comparative representation of the Raman spectra for the MB, MBA, and 5MB interphase (the 50th spectrum in Fig. 4).

and band enhancement) prevented us from quantification of the tetragonal and trigonal boron atoms proportions. Other dissimilarity between intergrains phase of the 5MB and MBA consists in the relative intensities of the main band in the MF region and the broad band in the HF region. More intense asymmetric band peaking up at about 802 cm^{-1} than the band peaking up at about 1345 cm^{-1} in case of the 5MB composite signals higher content in superstructural units like rings (730–770 cm^{-1}) than loose or broken superstructural units with bands within 490–570 cm^{-1} and 1340–1550 cm^{-1}, respectively.

In contrast to the grain phase where Ti in rutile adopted octahedral coordination (TiO_6), the spectrum of the intergrains phase has a new band at about 896 cm^{-1} (see Table 5), assignable to TiO_4 units. This means the amount of TiO_2 inserted in the borate matrix is relatively small [28], less than 5 wt%, otherwise higher coordinated titanium units are expected to be formed and to give Raman bands at lower frequencies in the 600–650 cm^{-1} range [33]. This arises from the fact that stronger *Me*–O bond (where *Me* can be Ti and/or Al) in a lower coordination group gives Raman bands at frequencies higher than those given by *Me*–O bonds in higher coordination group [33].

Finally, distinct structure of the intergrains phase of the composite under discussion in comparison to the blank sodium aluminum borate glass is also trigged by TiB_2 formation and/or incomplete SHS reactions. Formation of Al_2O_3 during SHS preparation, difficult to infer from the Raman data due to the band overlapping with the borate matrix, seems to inhibit the growth of coarse-grained microstructure in TiB_2-composites and hence the obtaining of dense composites with improved properties, especially wear resistance [31].

Micro-Raman results point out the formation of TiB_2 phase in conjunction with rutile in the grain phase both being accommodated in the newly formed sodium aluminum metaborate matrix, which also contain low quantity of the TiO_4 units. Mostly raw anatase underwent polymorphic transition to rutile, where Ti is 6-fold coordinated by oxygen atoms. Smaller amounts converted to TiB_2 compound by self-propagating synthesis and entered the borate network as TiO_4.

3.2. XPS spectra

The spectra of the 2MB and 5MB composites, illustrated in Fig. 6, show strong signals from Al, B, C, O, and Na, and a weak peak from Ti. Results of the spectra integration are listed in Tables 6 and 7. The C is ascribed to C–C, C–O, O–C=O, and carbonate bonding schemes [18,34] originates from sample preparation and manipulation (Table 6).

The B1s band at about 192 eV is from oxidized boron, presumably from B_2O_3, with long B–O bondings [35] due to the higher atomic ratio B/Ti than 20, as seen in Table 6. In the same

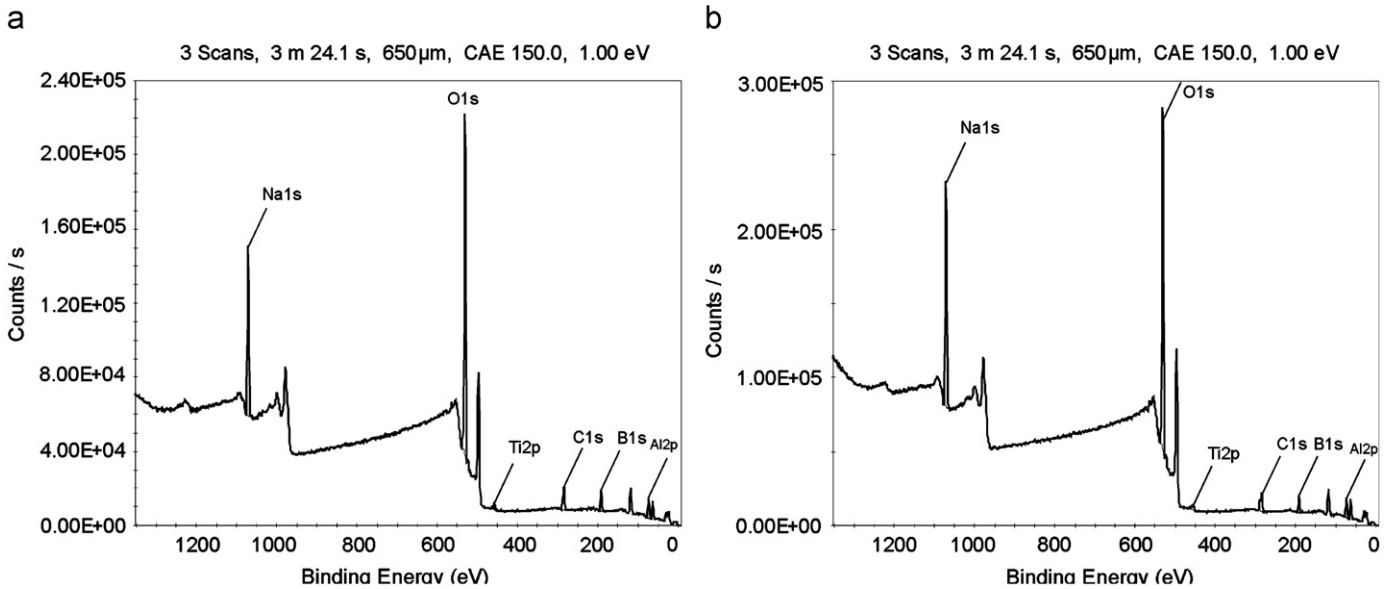

Fig. 6. XPS survey spectra of (a) 2MB and (b) 5MB composites.

Table 6
XPS parameters of the two composites 2MB and 5MB.

Peak	2MB			5MB		
	BE (eV)	FWHM	Atomic %	BE (eV)	FWHM	Atomic %
Al2p	73.65	1.72	14.56	73.85	1.83	14.61
B1s	191.89	1.54	16.69	191.82	1.52	14.10
C1s-CC	284.75	1.42	6.27	284.84	1.51	4.71
C1s_CO	286.27	1.50	1.39	286.84	1.50	1.18
C1s_COO	288.36	1.43	1.03	288.40	1.1	0.51
C1s-carbonate	289.61	1.36	0.96	289.65	1.50	2.24
Ti2p	458.01	1.62	0.57	457.92	1.48	0.43
O1s	531.22	1.89	46.52	531.25	1.78	47.42
Na1s	1071.80	2.24	12.01	1071.73	2.15	14.80
			B/Ti=29.28			B/Ti=32.79

Table 7
Parameters of the Ti2p region of the 2MB and 5MB.

Peak	2MB			5MB		
	BE (eV)	FWHM	Atomic %	BE (eV)	FWHM	Atomic %
Ti2p3–Ti^0	453.70	1.26	3.40	453.8	1.10	18.50
Ti2p3–TiB_2	454.60	1.15	3.30	454.6	1.10	6.60
Ti2p3–$TiO_{2-x}B_x$	455.84	1.2	6.70	455.6	1.35	10.60
Ti2p3–TiO_2	458.00	1.70	86.6	457.9	1.70	64.30

work [35] on the B-doped TiO_2 photocatalysts, formation of B_2O_3 which covers and inhibits crystal size of TiO_2 was noticed at big B/Ti ratio. Other close binding energies of 191.6, 190.6, and 193 eV belong to Ti–O–B (first one) and O–Ti–B bonds [36], respectively.

The XPS spectra of the O1s region of both samples investigated, 2MB and 5MB, located at 531.25 eV originates from anion doped TiO_2-containing materials typically located from 530 to 534 eV [37]. Such energy was prior reported for $TiO_{2-x}B_x$ compounds [38]. Oxygen in hydroxyl group gives an XPS peak at 531.4 eV [35]. In oxidic glasses, as borate glasses, two types of oxygen atoms exist, non-bridging and bridging ones, and they give a single XPS peak with asymmetric shape [39]. The non-bridging oxygen gives a signal with lower binding energy (BE), below 531 eV. If the BE of the O1s region slightly decrease from 5MB to 2MB, the BE of the Na1s region (Table 6) has opposite trend and signals increased ionicity of the *M*–O bonds (where *M* is B and/or Ti) in 2MB. However, higher ionicity is expected in the glassy systems with higher Na_2O content which is conflicting with the richer Na content of the 5MB composite (Table 6). The plausible explanation consists in the fact that Na_2O is not the only glass modifier of the B_2O_3 structure.

Although there is a single peak from Al2p, its asymmetric shape towards the high energy side (above 75 eV) might include contributions of the Al^{3+} as modifier and glass former, AlO_6 and AlO_4, respectively, analogous to the literature data on Al2p peaks located at 77.9 and 78.5 eV in aluminum silicate glasses [40].

The Ti2p spectra (Fig. 7) acquired with a high energy pass enabled us to deconvolute them into four components. The highest peak, at 457.8 eV, is highly oxidized, and has been attributed to TiO_2 [37]. Between them, two additional peaks are required to indicate TiB_2 and some variable oxidation of the original Ti boride. The latter state, termed TiB_xO_{2-x}, indicates incomplete Al reducing TiO_2 and B_2O_3 as well as slightly oxidized boride during sample preparation. These peak positions are consistent with nearly six-fold coordinated titanium ions [37]. According to the fitting results (see Table 7) higher content in metallic Ti and TiB_2 and lower TiO_2 content of the 5MB material was noticed contrary to the predicted content by the reactions in Table 1. Giving the fact that sodium borate glasses are used in recovery of Ti from alloys and refining Al–Ti–B grains [41] higher $Na_2B_2O_4$ content of the 5MB composite can trigger formation of a higher quantity of Ti^0. Due to the reduced Ti content (Table 6) within 5 nm detection limit of the spectrometer, we can conclude that XPS measurements targeted mostly the intergrains phase. Therefore, more extensive XPS investigations (depth profile) are due to investigate grain phase and/or confirm the core-shell model forwarded by Vallauri et al. [3] for TiB_2–TiC composites.

4. Conclusion

This work presents the structural characterization of two TiB_2–metaborate composites obtained by self-propagating high-temperature synthesis, 2MB and 5MB, using Raman and X-ray photoelectron spectroscopies. Results were discussed according to the grain and intergrains phases and compared with commercial

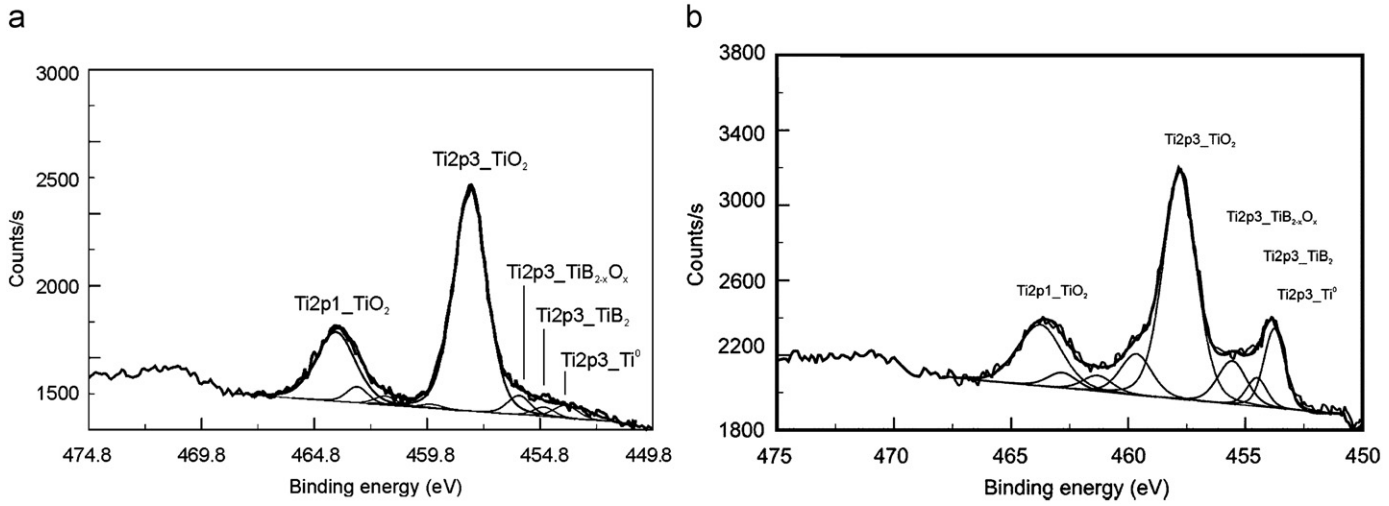

Fig. 7. Deconvoluted Ti2p XPS spectra for the 2MB and 5MB composites (50 scans, 11 min 17 s, 650 μm, CAE 40.0, 0.10 eV).

TiB_2 and the blank borate matrix. Thus, the grain phase of the two composites consists of rutile (TiO_2) and TiB_2, which indicates that the SHS reaction was not completed. Different proportion of TiB_2 and rutile obtained from Raman and XPS data are generated by the fact that both techniques micro-Raman and XPS have different penetration depth, higher in the case of Raman spectroscopy. However, higher proportion of TiB_2 was derived by spectral integration of the Raman spectrum of the 5MB grain phase in comparison to the 2MB grain, respectively.

In-line Raman spectra showed uneven distribution of prismatic grains in the borate matrix. Also the intergrains phase, or metaborate matrix, was found less disordered (narrower and split Raman bands) than the blank MBA ($Na_2B_2O_4 \cdot Al_2O_3$). The constrained-width model for the spectral deconvolution of the high-frequency Raman band, forwarded to compare results with the quantitative NMR data in literature, was successful in estimating the proportion of the tetrahedral boron atoms, N_4, of the blank MBA. However, it failed to produce reasonable results for the intergrains phase. This is due to the presence of unreacted materials: small amounts of TiO_2 (less than 5 wt%) and graphitic materials. Despite the comparable amount of Na_2O used in preparation of the two composites, 20.01% in case of 2MB and 22.51% for 5MB, increased ionicity of the *M*–O bonds (*M* is B and/or Ti) was signaled by XPS data for 2MB due to higher content of the unreacted TiO_2.

Acknowledgments

This work was partially supported by Romanian Academy, Czech Academy of Science cooperation. The authors thank Dr. I. Gregora for the fitting procedure for the Raman spectra and enlightening discussions. One of the authors (EB) acknowledges financial support from ASCR (Project AVOZ10100520).

References

[1] P. Peshev, S. Peshev, V. Nikolov, P. Gravereau, J.-P. Chaminade, D. Binev, D. Ivanova, J. Non-cryst. Solids 179 (2006) 2834–2849.
[2] G. Corbel, D. Mazza, O. Bohnke, M. Leblanc, Solid State Sci. 7 (2005) 588–593.
[3] D. Vallauri, I.C. Atıas Adrian, A. Chrysanthou, J. Eur. Ceram. Soc. 28 (2008) 1697–1713.
[4] H.C.Yi, J.Y.Guigne, J.J.Moore, US Patent 5,792,417, 1998.
[5] H.C.Yi, J.Y.Guigne, J.J.Moore, U.S. Patent 6,645,424, 2003.
[6] H. Zhu, H. Wang, L. Ge, S. Chen, S. Wu, Trans. Nonferous Met. Soc. China 17 (2007) 590–594.
[7] A.K. Khanra, M.M. Godkhindi, J. Am. Ceram. Soc. 88 (2005) 1619–1621.
[8] G.K. Abdullaev, P.F. Rza-Zade, Kh.S. Mamedov, Zh. Neorg. Khim. 28 (1983) 208–211.
[9] S.W. Martin, E.I. Cooper, C.A. Angell, J. Am. Ceram. Soc. 66 (1983) 153–154.
[10] R. Akagi, N. Ohtori, N. Umesaki, J. Non-cryst. Solids 293–295 (2001) 471–476.
[11] L. Robinet, A. Bouquillon, J. Hartwig, J. Raman Spectrosc. 39 (2008) 618–626.
[12] M.T. Anthony, in: D. Briggs, M.P. Seah (Eds.), Practical Surface Analysis, Auger and X-ray Photoelectron Spectroscopy, vol 1, Wiley, Chichester, 1990.
[13] Y. Yu, J.-H. Yu, G. Xiong, C. Li, F.-S. Xiao, Phys. Chem. Chem. Phys. 3 (2001) 2692–2696.
[14] G.D. Chryssikos, M.S. Bitsis, J.A. Kapoutsis, E.I. Kamitsos, J. Non-cryst. Solids 217 (1997) 278–290.
[15] E.I. Kamitsos, M.A. Karakassides, Phys. Chem. Glasses 30 (1989) 19–26; G.D. Chryssikos, J.A. Kapotsis, E.I. Kamitsos, A.P. Patsis, A.J. Pappin, J. Non-cryst. Solids 167 (1994) 92–105.
[16] J. Fukunaga, R. Ota, J. Non-cryst. Solids 95 (1987) 270–278.
[17] E.I. Kamitsos, M.A. Karakassides, G.D. Chryssikos, J. Phys. Chem. 91 (1987) 1073–1079.
[18] M. Hassan, R.S. Rawat, P. Lee, S.M. Hhassan, A. Gayyum, R. Ahmad, G. Murtaza, M. Zakaullah, Appl. Phys. A 90 (2008) 669–677.
[19] G.D. Chryssikos, J.A. Kapoutsis, A.P. Patsis, E.I. Kamitsos, Spectrochim. Acta 47A (1991) 1117–1126.
[20] M. Bertmer, L. Zuchner, J.C.C. Chan, H. Eckert, J. Phys. Chem. B. 104 (2000) 6541–6553.
[21] T. Yano, N. Kunimine, S. Shibata, M. Yamane, J. Non-cryst. Solids 321 (2003) 137–146.
[22] E.M. Anghel, P. Florian, C. Bessada, J. Phys. Chem. B 111 (2007) 962–967.
[23] W.L. Konijnendijk, J.M. Stevels, J. Non-cryst. Solids 18 (1975) 307–331.
[24] L. Cormier, O. Majerus, D.R. Neuville, G. Calas, J. Am. Ceram. Soc. 89 (2006) 13–19.
[25] B.G. Parkinson, D. Holland, M.E. Smith, A.P. Howes, C.R. Scales, J. Phys.: Condens. Matter 19 (415114) (2007) 1–12.
[26] S.K. Lee, M. Dechamps, J. Hiet, D. Massiot, S.Y. Park, J. Phys. Chem. B 113 (2009) 5162–5167.
[27] T.J. Kiczenski, L.-S. Du, J.F. Stebbins, J. Non-cryst. Solids 337 (2004) 142–149.
[28] P. Florian, E.M. Anghel, C. Bessada, J. Phys. Chem. B 111 (2007) 968–978.
[29] L. Zuchner, J.C.C. Chan, W. Muller-Warmuth, H. Eckert, J. Phys. Chem. B 102 (1998) 4495–4506.
[30] L. Baca, N. Stelzer, J. Eur. Ceram. Soc. 28 (2008) 907–911.
[31] I. Burlacov, J. Jirkovsky, M. Muller, R.B. Heimann, Surf. Coat. Technol. 201 (2006) 255–264.
[32] R.E. Youngman, J.W. Zwanziger, J. Phys. Chem. 100 (1996) 16720–16728.
[33] S. Sakka, F. Miyaji, K. Fukumi, J. Non-cryst. Solids 112 (1989) 64–68.
[34] M. Ni, B.D. Ratner, Surf. Interface Anal. 40 (2008) 1356–1361.
[35] D. Chen, D. Yang, Q. Wang, Z. Jiang, Ind. Eng. Chem. Res. 45 (2006) 4110–4116.
[36] G. Liu, Y. Zhao, C. Sun, F. Li, G.Q. Lu, H.-M. Cheng, Angew. Chem. Int. Ed. 47 (2008) 4516–4519.
[37] E.A. Reyes-Garcia, Y. Sun, D. Raftery, J. Phys. Chem. B 111 (2007) 17146–17154.
[38] Z.-L. Jin, G.-X. Lu, Energy Fuels 19 (2005) 1126–1132.
[39] D. Raskar, M.T. Rinke, H. Eckert, J. Phys. Chem. C 112 (2008) 12530–12539.
[40] R.G. Duan, K.-M. Liang, S.-R. Gu, Mater. Sci. Eng. A 249 (1998) 217–222.
[41] Y. Birol, J. Alloys Compd. 458 (2008) 271–276.